

# The electrocaloric effect in BaTiO<sub>3</sub> at all three ferroelectric transitions: anisotropy and inverse caloric effects

Madhura Marathe,<sup>1,\*</sup> Damian Renggli,<sup>1</sup> Mehmet Sanlialp,<sup>2</sup> Maksim O. Karabasov,<sup>2</sup> Vladimir V. Shvartsman,<sup>2</sup> Doru C. Lupascu,<sup>2</sup> Anna Grünebohm,<sup>3</sup> and Claude Ederer<sup>1,†</sup>

<sup>1</sup>*Materials Theory, ETH Zürich, Wolfgang-Pauli-Str. 27, 8093 Zürich, Switzerland*

<sup>2</sup>*Institute for Materials Science and Center for Nanointegration Duisburg-Essen (CENIDE), University of Duisburg-Essen, 45141 Essen, Germany*

<sup>3</sup>*Faculty of Physics and Center for Nanointegration Duisburg-Essen (CENIDE), University of Duisburg-Essen, 47048, Duisburg, Germany*

(Dated: August 29, 2018)

We study the electrocaloric (EC) effect in bulk BaTiO<sub>3</sub> (BTO) using molecular dynamics simulations of a first principles-based effective Hamiltonian, combined with direct measurements of the adiabatic EC temperature change in BTO single crystals. We examine in particular the dependence of the EC effect on the direction of the applied electric field at all three ferroelectric transitions, and we show that the EC response is strongly anisotropic. Most strikingly, an inverse caloric effect, i.e., a temperature increase under field removal, can be observed at both ferroelectric-ferroelectric transitions for certain orientations of the applied field. Using the generalized Clausius-Clapeyron equation, we show that the inverse effect occurs exactly for those cases where the field orientation favors the higher temperature/higher entropy phase. Our simulations show that temperature changes of around 1 K can in principle be obtained at the tetragonal-orthorhombic transition close to room temperature, even for small applied fields, provided that the applied field is strong enough to drive the system across the first order transition line. Our direct EC measurements for BTO single crystals at the cubic-tetragonal and at the tetragonal-orthorhombic transitions are in good qualitative agreement with our theoretical predictions, and in particular confirm the occurrence of an inverse EC effect at the tetragonal-orthorhombic transition for electric fields applied along the [001] pseudo-cubic direction.

## I. INTRODUCTION

The electrocaloric (EC) effect – a reversible temperature change of a material under adiabatic application or removal of an electric field – was first reported in 1930.<sup>1</sup> While initially the effect was considered too weak to be useful for applications, technological applications are now considered feasible, after a very large EC temperature change of  $\sim 12$  K has been reported for thin films of PbZr<sub>0.95</sub>Ti<sub>0.05</sub>O<sub>3</sub>.<sup>2</sup> This observation has led to a large increase in research activity on the EC effect.<sup>3–5</sup> The EC effect, as well as the analogous magnetocaloric and elastocaloric effects, which can be observed in certain materials under application of a magnetic field or a stress field, respectively,<sup>6,7</sup> are currently attracting considerable attention. All three caloric effects can facilitate the development of a new generation of solid state cooling devices, which promise to be more energy-efficient and environmentally-friendly than currently existing devices based on vapor compression.<sup>8,9</sup>

In the present work, we focus on BaTiO<sub>3</sub> (BTO), which is a well-characterized prototypical ferroelectric (FE) material. BTO exhibits a paraelectric (PE) cubic (C) phase at high temperature, which on cooling transforms into a FE tetragonal (T) phase at  $\sim 120^\circ\text{C}$ . Further cooling leads to two FE-FE transitions, first to an orthorhombic (O) phase at  $\sim 5^\circ\text{C}$  and finally to a rhombohedral (R) phase at  $\sim -90^\circ\text{C}$ .<sup>10</sup> In each FE phase, the spontaneous electric polarization points along a different crystallographic direction. The strongest EC effect is typically

observed in FE materials close to a FE phase transition, where application of a moderate electric field can result in very large changes of the electric polarization.<sup>4</sup> Therefore, the various transitions make BTO a very attractive system for exploring the EC effect.

The EC effect in BTO has been studied both experimentally, see e.g., Refs. 11–13, as well as theoretically, using either phenomenological thermodynamical modeling or an *ab initio*-based effective Hamiltonian approach, see e.g., Refs. 14–20. Most of these previous studies have focused on the temperature region around the PE-FE transition, where particularly large field-induced polarization changes occur. However, large polarization changes, including reorientation of the polarization direction along different crystallographic axes, also occur at the FE-FE transitions. Indeed, an EC effect corresponding to a temperature change of 1.4 K under application of an electric field of 10 kV/cm has been reported at the T-O transition in BTO.<sup>21</sup> Furthermore, *ab initio*-based studies predict sizable EC temperature changes both at the T-O and at the O-R transition in BTO,<sup>18</sup> as well as in the closely related compound Ba<sub>0.5</sub>Sr<sub>0.5</sub>TiO<sub>3</sub>.<sup>22</sup> A finite EC response has also been measured at FE-FE transitions in other ferroelectrics, e.g., Pb(Mg<sub>1/3</sub>Nb<sub>2/3</sub>)O<sub>3</sub>-PbTiO<sub>3</sub> single crystals.<sup>23</sup>

Generally, the EC effect is related to the polarization change along the direction of the applied field, and thus most theoretical studies have considered an electric field applied along the direction of the spontaneous polarization in the FE phase. Nevertheless, some experimental

studies have been performed for Pb-based relaxor single crystals grown with different orientations,<sup>24–26</sup> and have confirmed that the EC response indeed depends on the orientation of the applied field. This *anisotropy* of the EC effect has not received much attention so far. In the case of a FE-FE transition for which the orientation of the spontaneous polarization changes between two crystallographically inequivalent directions, the anisotropy of the EC effect is particularly relevant, and is currently not fully understood.

Remarkably, an *inverse* (or negative) EC response, i.e., a temperature decrease under application of an electric field, has been observed for certain applied field directions within a small temperature region.<sup>23</sup> Ponomareva and Lisenkov have attributed this inverse EC effect to noncollinearity between the electric polarization and the applied field, and were able to reproduce the inverse effect in their *ab initio*-based simulations.<sup>22</sup> However, a full understanding of this inverse EC effect and the conditions required for observing it at FE-FE transitions is still lacking.

Due to its multiple FE transitions, BTO is an ideal system to develop a better general understanding of the EC response at FE-FE transitions, of the corresponding anisotropy, and of a possible inverse EC response. We note that the first FE-FE (T-O) transition in BTO occurs just below room temperature, and thus in a very attractive temperature region for many anticipated technological applications. Furthermore, modified EC cycles have been suggested which could enhance the overall EC response of a material by utilizing a combination of normal and inverse EC effects.<sup>22,27</sup>

In this paper, we present a detailed and systematic study of the EC effect in BTO at all three FE transitions using a first principles-based effective Hamiltonian approach. In particular, we examine how the direction of the applied field affects the EC temperature change. Since application of an external electric field shifts the phase transition temperatures and can also affect the order of the corresponding phase transition, we first establish the electric-field versus temperature phase diagram for different orientations of the electric field. We obtain a finite adiabatic EC temperature change at all three transitions. For some field orientations an inverse EC effect can be observed at the FE-FE transitions, and we analyze the mechanism leading to such inverse effects in terms of the Clausius-Clapeyron equation. To verify our theoretical predictions and the results of our simulations, we also perform direct measurements of the EC temperature change in BTO single crystals along different crystallographic directions. We observe good qualitative agreement between our simulations and the experimental measurements.

This paper is organized as follows. In Secs. II and III, we describe our computational and experimental methods, respectively. We then present and discuss the calculated electric field versus temperature phase diagrams (Sec. IV A), followed by the discussion of potential inverse

caloric effects using the generalized Clausius-Clapeyron equation, along with an estimation of the entropy changes associated with the latent heat of the various first-order phase transitions (Sec. IV B). Next, we present the calculated EC temperature changes for different applied field directions, and we also discuss some examples of non-monotonic behavior of the EC temperature changes as function of the electric field magnitude (Sec. IV C). Finally, in Sec. IV D we present the directly measured EC temperature changes for BTO single crystals corresponding to different orientations of the applied field, and we summarize our results in Sec. V.

## II. COMPUTATIONAL METHOD

We use a first principles-based effective Hamiltonian approach,<sup>28,29</sup> which is applicable to FE materials exhibiting a cubic perovskite structure at high temperatures. Within this approach, only those degrees of freedom are considered that are essential to correctly describe the FE transitions. To this end, each cubic perovskite unit cell,  $i$ , is represented by a three-dimensional soft mode vector  $\mathbf{u}_i$  and a vector describing the local strain  $\mathbf{w}_i$ . Further, the global elastic degrees of freedom are included through the homogeneous strain tensor  $\eta_j$ ,  $j = 1, \dots, 6$  (in standard Voigt notation). The total energy of the system is then expressed as a low order polynomial in terms of these variables, and includes various terms describing the so-called soft-mode self energy (the tendency to form local dipoles), the dipole-dipole interaction energy, a short range interaction between soft modes, the homogeneous and inhomogeneous elastic energy, and additional terms describing the coupling between soft mode and strain variables. The latter are essential to correctly describe the three successive phase transitions in BTO and related materials. All parameters of this effective Hamiltonian can be calculated using *ab initio* density functional theory,<sup>29,30</sup> i.e., no empirical fitting to experimental data is required.

We use the open-source “feram” code (<http://loto.sourceforge.net/feram/>)<sup>31</sup> to perform molecular dynamics (MD) simulations for this effective Hamiltonian, allowing us to access finite temperature properties. Further, we use the previously reported parameter set for bulk BaTiO<sub>3</sub>,<sup>30</sup> determined using density functional theory calculations with the Wu-Cohen exchange-correlation functional.<sup>32</sup> A  $96 \times 96 \times 96$  supercell is used in all our simulations, corresponding to about 900 000 perovskite units. The system is equilibrated at a given temperature, with or without applied field, within the canonical, i.e., “constant temperature” (NPT) ensemble using a Nosé-Poincaré thermostat.<sup>33</sup>

The transition temperatures for the FE phase transitions at a fixed applied electric field are determined sequentially by performing both “heating” and “cooling” simulations, i.e., each simulation is initialized using a previously thermalized configuration obtained at slightly

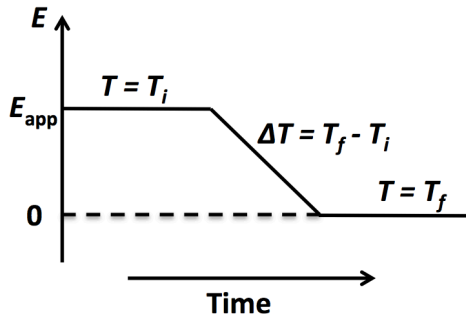


FIG. 1. Schematic representation of the computational protocol used to obtain the adiabatic temperature change for switching the field off. Here,  $E_{\text{app}}$  is the applied field.  $T_i$  and  $T_f$  denote initial and final temperatures corresponding to  $E_{\text{kin}}^i$  and  $E_{\text{kin}}^f$ , respectively.

lower or higher temperature, respectively. We use temperature steps of 10 K far away from a phase transition and reduced steps of 2 K near phase transitions. The system is thermalized over a time period of 120 ps, and then statistical averages for various quantities are accumulated over a period of 160 ps, using MD time steps of 2 fs.

To determine the adiabatic temperature change under application or removal of an external electric field, we employ the microcanonical, i.e., “constant energy” (NPE) ensemble after the system has been thermalized at a given temperature and field. This allows us to monitor the change in kinetic energy of the system while the electric field is slowly ramped up or down. The EC temperature change  $\Delta T$  is then obtained using:

$$\Delta T = \frac{2(E_{\text{kin}}^f - E_{\text{kin}}^i)}{N_f k_B}. \quad (1)$$

Here,  $E_{\text{kin}}^i$  and  $E_{\text{kin}}^f$  denote the initial and final average kinetic energies of the system,  $N_f$  is the number of degrees of freedom of the model system, and  $k_B$  is the Boltzmann constant. The computational protocol is schematically shown in Fig. 1. Except where otherwise noted, the applied electric field along each Cartesian direction is changed with a rate 0.002 kV/(cm·fs), which is slow enough to ensure that the system remains in thermal equilibrium during the field ramping.<sup>34</sup> The system is thermalized before and after the ramping for 80 ps, and then thermal averages are accumulated over a period of 40 ps (before the field ramping) and 100 ps (after the field ramping). A MD time step of 1 fs is used for these simulations.

We note that, for computational efficiency, only the soft mode variables are treated as dynamical variables within this work, whereas the local and global strain variables are obtained by minimizing the total energy for the current soft mode configuration in each MD step. Thus, our simulations contain only 3 dynamical (fluctuating)

variables per perovskite unit cell, as compared to 15 in the real material. As a result, the specific heat of the model system is smaller than that of the real material by approximately a factor of  $3/15 = 1/5$ . Consequently, the calculated  $\Delta T$  is overestimated by approximately a factor of 5, and in the following we always report “scaled”  $\Delta T$  values, which are corrected by this factor to match our values to the number of degrees of freedom of the real system.<sup>18</sup> In contrast, whenever we report absolute temperature values, these correspond to the actual system temperature  $T$  of our model system during the simulation. In this case, rescaling is not applicable.

Further, we note that, while the effective Hamiltonian approach is able to successfully reproduce all three FE transitions in BTO,<sup>29,30</sup> the calculated transition temperatures deviate by some amount from the experimentally measured values. These deviations result from the simplifications inherent in the effective Hamiltonian method (reduced number of variables, neglect of higher order terms in the total energy) as well as from the approximations used to calculate the corresponding parameters using density functional theory.<sup>35</sup> While some of these deviations can be reduced by using either fixed or temperature-dependent pressure corrections (see, e.g., Refs. 29 and 30), in the present work we do not use such empirical corrections, since their applicability is not apparent if the temperature of the system varies during the simulation.<sup>18</sup> We point out that the effective Hamiltonian approach was shown to be a powerful method that allows to obtain general understanding and give crucial information on overall magnitudes as well as expected trends.

### III. EXPERIMENTAL METHOD

BTO single crystals (3 mm × 3 mm × 0.5 mm) cut perpendicular to the [001], [011] and [111] directions, were purchased from EQ Photonics GmbH. For electrocaloric measurements they were sputtered with 100 nm Au electrodes on both faces. We note that here and in the following, we always use cubic (or pseudo-cubic) notation to specify the crystallographic directions, i.e. [100], [010], and [001] correspond to the Cartesian  $x$ ,  $y$ , and  $z$  directions.

The EC effect was directly measured using a custom-built quasi-adiabatic calorimeter under high vacuum-condition (about  $10^{-6}$  mbar). The measurements were performed on heating between 276 K and 420 K. Electric field pulses with magnitudes of 5, 7.5, and 10 kV/cm, and a period of 200 s, were applied at each measurement temperature. For each temperature and field value, four temperature changes were measured over two field cycles (i.e., two measurements for switching on and two for switching off the field). From this data, the mean EC temperature change and the corresponding standard deviation were obtained. The electrical pulses were generated by a functional signal generator (Keith-

ley Model 3390) and amplified by a high-voltage amplifier (TREK Model PD05034). The sample temperature change,  $\Delta T_{\text{meas}}$ , was recorded by a Kapton<sup>®</sup> - insulated type K thermocouple, contacted to the top electrode of the sample and connected to a temperature controller (Lakeshore Cryotronics Model 336). The EC temperature change was then calculated taking into account the geometry of the system and the heat capacities of its components:

$$\Delta T = \Delta T_{\text{meas}} \sum_i \frac{C_p^i}{C_p^{EC}}. \quad (2)$$

Here,  $C_p^i$  represent the heat capacities of each subsystem  $i$  (parts of the sample with electrode and without electrode, electrical wires, alumina compound to contact the thermocouple, silver paste to fix the electrical wires) which are in contact with the sample, and  $C_p^{EC}$  is the heat capacity of the BTO single crystal covered by the electrode.<sup>36</sup> Both the heat capacity and the phase transition temperatures of the BTO single crystals were measured using a differential scanning calorimeter (Netzsch, DSC 204) on heating and on cooling at 10 K/min over a temperature range of 250-425 K, as reported elsewhere.<sup>37</sup>

## IV. RESULTS AND DISCUSSION

### A. $E$ - $T$ phase diagrams

We first examine how the magnitude as well as the direction of an applied electric field alters the nature of the different phases and the corresponding phase transition temperatures in bulk BaTiO<sub>3</sub>. We consider three different field directions: [001], [011], and [111], which correspond to the directions of the spontaneous polarization in the T, O, and R phases, respectively. We determine the phase transition temperatures from the temperature dependence of the different polarization components calculated during heating and cooling simulations. As example, different components of the polarization,  $P_\alpha$ ,  $\alpha \in \{x, y, z\}$ , are plotted as a function of temperature for a few applied fields in Fig. 2. For brevity, we only show data from cooling simulations. The data obtained from heating simulations is analogous, except that the resulting transition temperatures are typically somewhat higher than the ones obtained from the cooling simulations. This is due to the thermal hysteresis associated with the first order phase transitions. Note that here and in the following, we usually specify the magnitude  $E_\alpha$  for each nonzero component of the applied field, i.e., the corresponding fields  $\vec{E}$  are  $(0, 0, E_\alpha)$ ,  $(0, E_\alpha, E_\alpha)$ , and  $(E_\alpha, E_\alpha, E_\alpha)$  for fields applied along [001], [011], and [111], respectively.

For zero electric field, sharp jumps can be observed in the different polarization components at the transition temperatures (see black lines in Fig. 2), indicating the first order (discontinuous) character of each transition,

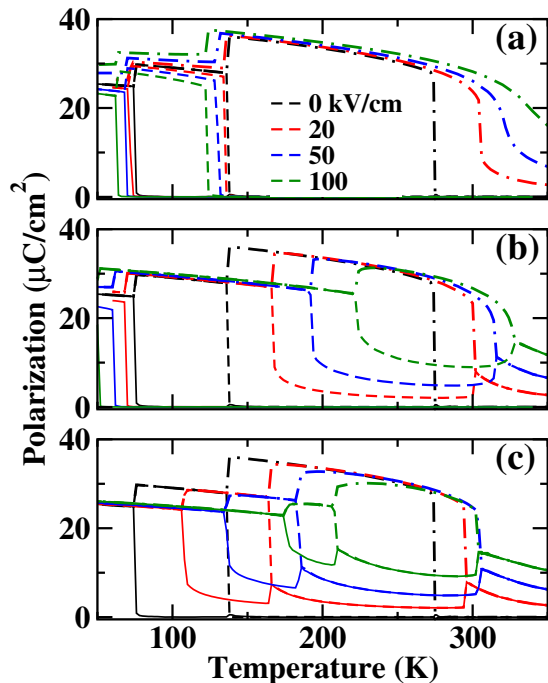


FIG. 2. Polarization components along  $x$  (solid lines),  $y$  (dashed lines), and  $z$  (dot-dashed lines) directions are plotted as a function of temperature for several electric fields applied along (a) [001], (b) [011] and (c) [111]. For clarity, only the results obtained from cooling simulations and for selected field strengths  $E_\alpha$  are shown.

as expected for bulk BTO.<sup>10</sup> With decreasing temperature, one can observe successive transitions from the PE-C phase to the FE-T, O, and R phases, corresponding to one, two, and three nonzero Cartesian components of the polarization, respectively.

Under application of an electric field, the transition temperatures shift to either lower or higher temperatures, depending on the specific transition and field direction. Simultaneously, in all cases where the electric field is not parallel to the zero-field polarization direction, the symmetry of the corresponding phase is reduced to monoclinic, due to non-zero polarization components induced by the applied field, or due to enhanced polarization components along the field direction. In spite of this symmetry-lowering, in the following we will continue to label the different FE phases as T, O, and R, i.e., according to their zero field symmetries. Furthermore, for each field direction the symmetry of the “PE” phase, becomes identical to the one of the FE phase that has its spontaneous zero-field polarization along the direction of the applied field.

The resulting electric field versus temperature ( $E$ - $T$ ) phase diagram is shown in Fig. 3. Each panel corresponds to the results obtained for a specific direction of the applied electric field. The shaded areas between heating and cooling curves corresponding to the same transition represent coexistence regions, where the observed phase

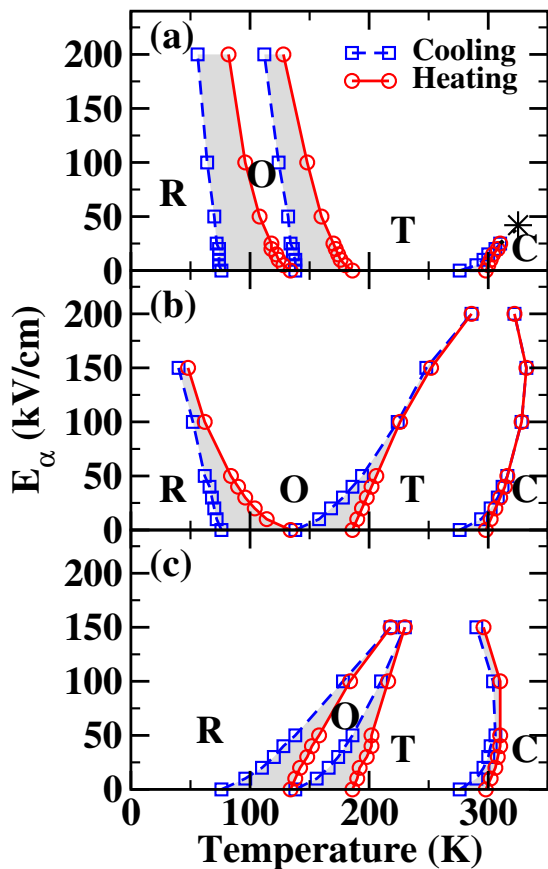


FIG. 3. Electric field versus temperature ( $E$ - $T$ ) phase diagram of BTO for fields applied along (a) [001], (b) [011], and (c) [111]. Here,  $E_\alpha$  is the magnitude of each non-zero Cartesian component of the applied field. Shaded regions between heating and cooling curves correspond to the coexistence regions between two phases. The black star in (a) indicates the estimated critical point ( $E_c, T_c$ ) for the PE-FE transition with field applied along [001].

of the system depends on its history. For all transitions and field directions, the width of the thermal hysteresis and thus the coexistence region decreases with increasing electric field. Note that we expect to obtain a more pronounced thermal hysteresis compared to what is typically observed in experiments, because our model system does not include any defects or inhomogeneities that can act as nucleation centers for the phase transition.

The overall structure of the  $E$ - $T$  phase diagram for the three different field directions agrees well with previous results obtained from thermodynamic modeling using Landau theory.<sup>38,39</sup> For each field direction, the temperature range of the FE phase which has its spontaneous polarization parallel to the applied field is strongly increasing with the field strength, and the corresponding transition lines shift to lower/higher temperatures, accordingly. All other phases will eventually vanish for sufficiently high field strength. However, the required fields for the R (R and O) phase(s) and field along [011]

([001]), i.e., the phase(s) on the low temperature side of the phase favored by the applied field, are much higher than our strongest applied electric fields. In contrast, the disappearance of the T phase for strong applied fields along [011] and [111] and of the O phase for strong applied fields along [111] can already be anticipated from the  $E$ - $T$  phase diagram shown in Fig. 3, even though the corresponding phase regions are not yet completely closed towards high  $E_\alpha$ .

For  $\vec{E} \parallel [001]$ , the first order transition emanating from the zero-field PE-C to FE-T transition ends in a critical point ( $E_c, T_c$ ), see, e.g., Ref. 13. This is because, as already mentioned, the symmetry of the “PE” phase<sup>40</sup> becomes identical to the one of the T phase for a field applied along [001]. Simultaneously, the applied field reduces the jump in  $P_z$  associated to the first order phase transition. Thus, once the temperature dependence of  $P_z$  becomes continuous, no phase transition occurs.

We can obtain a rough estimate for  $E_c$  and  $T_c$  by linearly extrapolating the jump in polarization obtained for small electric fields, i.e., where  $\Delta P$  is sizable, towards higher fields, and then identifying the field and temperature where this extrapolation becomes zero. In this way, we obtain a critical field around 40 kV/cm and a critical temperature around 325 K, which is indicated by the black star in Fig. 3(a). This value obtained for  $E_c$  is larger than what has been measured experimentally,<sup>13</sup> consistent with the expected stronger first order character of the transitions in our simulations compared to experiments (as already mentioned earlier). Nevertheless, we note that the thermal hysteresis of the corresponding PE-FE transition in our simulations essentially vanishes already for a field of around  $E_\alpha = 25$  kV/cm, and no clear jump in  $P_z(T)$  is recognizable any more above this field strength (see Fig. 2a). However, due to the limited numerical accuracy, finite-size effects, and the discretized  $T$ -sampling, it is not straightforward to identify the exact field strength at which  $P(T)$  becomes continuous from our data.

## B. Electrocaloric entropy change across the first order phase transitions

Following Refs. 41 and 42 we can obtain an expression for the isothermal electrocaloric entropy change,  $\Delta S = S(T, \vec{E}) - S(T, \vec{E} = 0)$ , under application of an external electric field,  $\vec{E}$ , across a first order phase boundary. For this, we express the field- and temperature-dependent polarization component along the field direction in the vicinity of a first order phase transition as follows:

$$P(T, E) = \tilde{P}(T, E) + \Delta P(E_t(T)) \Theta(T - T_t(E)). \quad (3)$$

Here,  $\tilde{P}(T, E)$  is the part of  $P$  that varies smoothly with  $T$  and  $E = |\vec{E}|$ ,  $\Delta P(E_t(T))$  is the jump in polarization at the temperature-dependent transition field



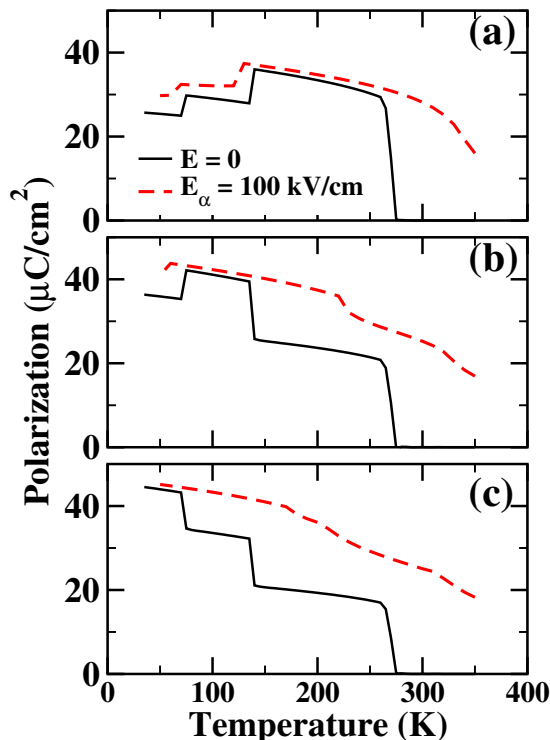


FIG. 4. Polarization projected along the field direction for different directions of the applied field – (a) [001], (b) [011], and (c) [111] – plotted as a function of temperature for zero field (black solid lines) and for  $E_\alpha = 100$  kV/cm (red dashed lines). We only show here results obtained during cooling simulations.

$E_t(T)$  (or, equivalently, at the field-dependent transition temperature  $T_t(E)$ ), and  $\Theta(T - T_t(E))$  is the Heaviside step function, which is 0 for  $T - T_t(E) < 0$  and 1 for  $T - T_t(E) > 0$ . Thus, positive (negative)  $\Delta P$  corresponds to the case where the polarization along the field direction is larger (smaller) above the transition temperature than below the transition temperature. Furthermore, we assume that  $E_t(T)$  and accordingly  $T_t(E)$  are uniquely defined in the considered temperature and field range.

Using the Maxwell relation  $(\partial S/\partial E)_T = (\partial P/\partial T)_E$ , where  $P$  refers to the polarization component along the direction of the applied field, and focusing only on the contribution to  $\Delta S$  resulting from the jump in  $P(T, E)$ , one obtains:

$$\Delta S = \Delta P(E_t(T)) \left| \frac{dE_t}{dT} \right|, \quad (4)$$

which corresponds to the well-known Clausius-Clapeyron equation.<sup>43</sup> From Eq. (4) it follows that the sign of the caloric entropy change when crossing a first order phase transition is determined by the sign of  $\Delta P(E_t(T))$ , i.e. the corresponding jump in the polarization along the direction of the applied field.

Fig. 4 shows the calculated polarization component along the field direction for different field directions as function of temperature and for two different field

strengths. It can be seen that both positive and negative  $\Delta P$  occurs at the T-O and O-R transitions, depending on the direction of the applied field. The polarization jumps are most pronounced for zero field, but are still qualitatively similar for  $E_\alpha = 100$  kV/cm. According to Eq. (4), a negative  $\Delta P$  corresponds to negative  $\Delta S$  and thus to a *normal* caloric effect, i.e., the entropy is decreased by the applied field. In contrast, positive  $\Delta P$  corresponds to positive  $\Delta S$  and thus gives rise to an *inverse* caloric effect, i.e., the applied field increases the entropy of the system.

Comparing Fig. 4 with Fig. 3, one realizes that the cases with positive  $\Delta P$  (T-O and O-R transitions for field along [001] and O-R transition for field along [011]), and thus with inverse caloric effect, correspond to the transitions and field directions with negative  $dE_t/dT$ , i.e., the cases where the applied field shifts the transition temperature to lower values. In these cases, if the electric field is increased under isothermal conditions, the phase transition line is crossed coming from the “low temperature phase” and entering into the “high temperature phase”, which is stabilized at the given temperature due to the applied field. Since the high temperature phase usually has the higher entropy, this means that  $\Delta S$  is positive, consistent with Eq. (4). Thus, Eq. (4) is crucial to understand the sign of the EC response at the FE-FE transitions, and both positive  $\Delta P$  and negative  $dE_t/dT$  indicate an inverse electrocaloric effect at the corresponding transition for a given field direction.<sup>44</sup> Note that the generalized Clausius-Clapeyron equation and its implications have already been discussed in the context of the magnetocaloric effect in shape memory Heusler alloys.<sup>41</sup>

We can also estimate the EC entropy change  $\Delta S$  associated with the first-order phase transition using our calculated field-dependent transition temperatures and polarization projections in Eq. (4). From the data shown in Fig. 3 we can extract  $dE_t/dT$  noting that  $T_t(E)$  is approximately linear at small fields ( $\leq 20$  kV/cm). We therefore obtain  $dE_t/dT|_{E=0}$  from a linear fit by using the average of  $T_t(E)$  calculated from heating and cooling simulations. We estimate the jump in polarization  $\Delta P|_{E=0}$  at each transition by averaging the data shown in Fig. 4 along with that obtained from the heating simulations. From Eq. (4) we then obtain  $|\Delta S(E = 0)| = 3.6$  J/kg/K for the PE-FE transition,  $|\Delta S(E = 0)| = 2.6$  J/kg/K for the T-O transition, and  $|\Delta S(E = 0)| = 1.4$  J/kg/K for the O-R transition. We note that these values are only rough estimates based on our data obtained for different field directions. Nevertheless, our estimates of  $\Delta S$  compare reasonably well with values of  $2.2 \pm 0.2$  J/kg/K measured in Ref. 12 for the C-T transition, and with  $2.4 \pm 0.2$  J/kg/K and  $2.2 \pm 0.2$  J/kg/K measured in Ref. 45 for the C-T and T-O transitions, respectively. A successive reduction of  $\Delta S$  for the C-T, T-O, and O-R transitions has also been reported in Ref. 46.

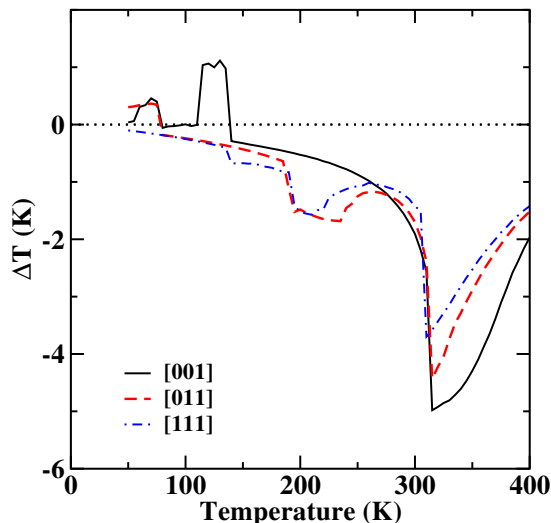


FIG. 5. EC temperature change under removal of an electric field, plotted as function of the initial temperature, for different field directions. For each direction the initially applied total field was  $E = 200$  kV/cm.

### C. Direct calculation of EC temperature change

Next, we directly calculate the adiabatic temperature change  $\Delta T$  for the three different field directions using the microcanonical ensemble, as described in Sec. II. In addition to the contribution resulting from the discontinuous jump ( $\Delta P$ ) at the phase transition, which was discussed in the previous subsection, the directly calculated  $\Delta T$  also includes the contribution to the EC response resulting from the smooth variation of  $P(T, E)$ , i.e.,  $\dot{P}(T, E)$  in Eq. (3).

The calculated  $\Delta T(T_i)$ , corresponding to removal of an electric field at initial temperature  $T_i$  is shown in Fig. 5 with the same total initial field  $E = |\vec{E}| = 200$  kV/cm applied along different directions. One can see that there are sharp features visible in  $\Delta T$ , corresponding to all three transitions, regardless of the direction of the applied field. The largest response is observed just above the zero-field PE-FE transition temperature, i.e., slightly above 300 K, with a maximum temperature change of around  $-5$  K for  $E = 200$  kV/cm applied along [001]. This is similar to what has been reported previously.<sup>18,22</sup> In the temperature range of the PE-FE transition and above, the calculated EC temperature change is qualitatively similar for all three directions for the applied field, but the magnitude of  $\Delta T$  depends strongly on the field direction and is largest (for the same total applied field) for  $\vec{E} \parallel [001]$ .

At lower temperatures, i.e., in the temperature range of the FE-FE transitions, there are pronounced qualitative differences between the three different field directions. In each case,  $\Delta T$  exhibits two rectangularly-shaped peaks corresponding to the T-O and O-R transitions, respectively. However, since the transition temperatures are

generally shifted in different ways for the different field directions, these peaks in  $\Delta T$  appear at different temperatures in each case. For  $\vec{E} \parallel [111]$  the two peaks are essentially merged into one single feature, since the two FE-FE transitions are very close in temperature.

Most strikingly, an *inverse* caloric effect, i.e., a positive  $\Delta T$  under field removal, can be observed at the T-O and O-R transitions for  $\vec{E} \parallel [001]$ , and at the O-R transition for  $\vec{E} \parallel [011]$ . These are exactly those cases where an inverse isothermal caloric entropy change has been predicted in the previous subsection based on Eq. (4) and the calculated jumps in polarization (Fig. 4). Thus, the qualitative considerations discussed in the previous subsection, which were based on Eq. (4), are consistent with the directly calculated temperature changes shown in Fig. 5.

We note that an earlier study has suggested that the inverse EC effect occurring close to a FE-FE phase boundary in  $\text{Ba}_{0.5}\text{Sr}_{0.5}\text{TiO}_3$  originates from noncollinearity between polarization and electric field.<sup>22</sup> Our results offer further clarification. In particular, one can see that  $\Delta T$  remains negative, i.e., “normal”, over the whole temperature range for  $\vec{E} \parallel [111]$ , in spite of the misalignment between the applied field and the polarization in both the T and O phases in this case. Thus, even if the applied field is not parallel to the polarization in any of the FE phases on either side of the transition, a normal EC effect can occur. The discussion in the previous section based on the Clausius Clapeyron equation offers a simple explanation of this, and shows that the crucial point is that the applied field induces a transition from a “low entropy” to a “high entropy” FE phase. While the noncollinearity between the field and the polarization direction in at least one of the FE phases is necessary to induce such a transition, the presence of the noncollinearity by itself is not sufficient to cause an inverse caloric effect.

In order to further analyze the occurrence of the inverse caloric effect, we now focus on the temperature region around the T-O transition for an applied field along the [001] direction, and we calculate the adiabatic EC temperature change at a fixed initial temperature but for different strengths of the applied electric field. In Fig. 6 we show the corresponding results for two different initial temperatures,  $T_i = 180$  K and  $T_i = 125$  K.

As seen from Fig. 3(a), at  $T_i = 180$  K, the T phase is stable over the whole range of applied field strengths, even for zero applied field. Consequently, the system is initially in the T phase and remains so under field removal. Fig. 6 shows that this results in a normal, i.e., negative, EC temperature change, the magnitude of which increases monotonously with increasing field strength.

In contrast, for an initial temperature of 125 K, the T phase is unstable for applied fields below  $\sim 90$  kV/cm, i.e., below the blue T-O transition line in Fig. 3(a). Thus, if for large applied fields the system is initially in the T phase it transforms into the O phase under field removal. As seen from Fig. 6, this results in a distinctly

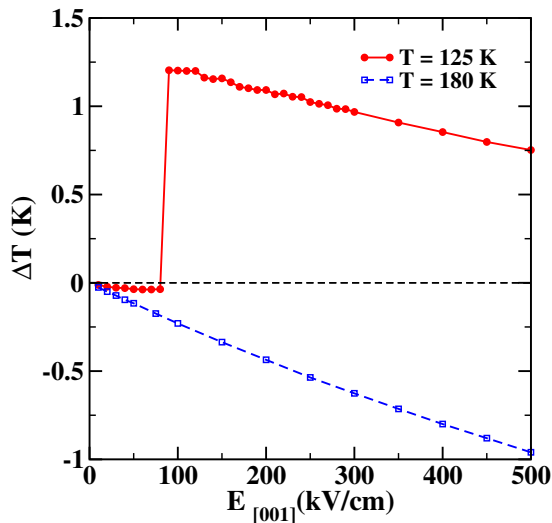


FIG. 6. Adiabatic EC temperature change,  $\Delta T$ , as function of the initially applied field magnitude for  $\vec{E} \parallel [001]$ . Each data point is calculated separately as the field is switched-off from the specified initial temperature, as shown schematically in Fig. 1.

non-monotonous dependence of  $\Delta T$  on the applied field strength. For small applied fields (below  $\sim 90$  kV/cm), the system is in the O phase both with and without applied field and exhibits a (rather small) normal EC effect (negative  $\Delta T$ ) that increases slightly with the field strength. However, once the applied field becomes larger than  $\sim 90$ - $100$  kV/cm, the system is initially in the T phase but then transforms into the O phase under field removal. This phase transition results in a strong inverse EC effect with a (positive) adiabatic temperature change of around 1.2 K, consistent with the negative (i.e. inverse) EC entropy change obtained from Eq. (4) for the T-O transition and field along [001]. If the magnitude of the applied field is further increased, then  $\Delta T$  decreases again, indicating a normal EC effect within the T phase. Thus, the inverse effect is indeed closely related to the T-O phase transition, as outlined in the previous subsection, and occurs exactly at the specific temperature-dependent transition field  $E_t(T)$  where the transition line is crossed.

Fig. 6 contains the *total*  $\Delta T$  under removal of a given initial field. To complement this, we can also plot the actual time evolution of the temperature (defined through the average kinetic energy) while we remove the field during the course of the simulation. This is shown, together with the evolution of the polarization components, in Fig. 7. The system is thermalized at  $T_i = 125$  K and an initially applied field of 200 kV/cm along [001]. It can be seen, that at the start of the simulation the system is in the T phase, with only one non-zero component of  $P$ . When the field is ramped down (between  $t = 200$  ps and  $t = 300$  ps), this component starts to decrease with the field, and simultaneously we observe a weak decrease in temperature, i.e., a normal EC effect. This confirms that

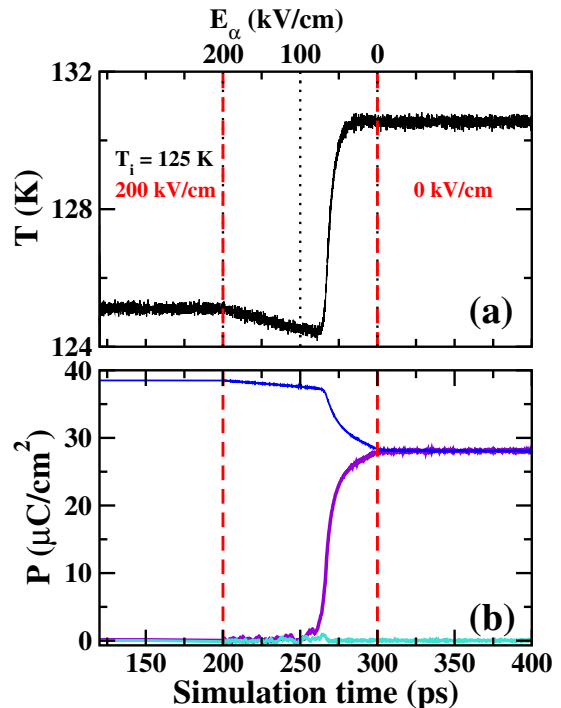


FIG. 7. Time evolution of the system temperature (a) and of the Cartesian components of the polarization (b) during the course of a simulation with an initial temperature of 125 K and an initial applied field of 200 kV/cm along [001]. Between  $t = 200$  ps and  $t = 300$  ps the applied field is ramped down to zero, as indicated on the top side of the graph.

the decrease of  $\Delta T$  observed in Fig. 6 for  $T_i = 125$  K and applied fields above 90 kV/cm is indeed related to the (relatively weak) normal EC effect within the T phase, that occurs while the initially applied field is ramped down to a value of around 90 kV/cm (see the evolution of  $T$  between  $t = 200$  ps and  $t = 250$  ps in Fig. 7).

However, once the field has decreased below 90 kV/cm, the T-O phase transition sets in, and the system starts to transform into the O phase, characterized by two equal non-zero polarization components. This transformation is accompanied by a sharp increase in temperature, corresponding to an inverse caloric effect. At the end of the field ramping phase ( $t = 300$  ps), the system has completely evolved into the O-phase and the overall change in temperature corresponds to an inverse EC effect.

As seen from Fig. 7, during the course of the phase transition, the system temperature in our simulation changes by about 6 K, which, after rescaling to the correct number of degrees of freedom, corresponds to  $\Delta T \approx 1.2$  K, consistent with the temperature change obtained from Fig. 6. It is important to note that, since this temperature change occurs exactly when the system is crossing the transition line, its magnitude is essentially independent of the strength of the initially applied electric field. The only requirement is that the applied field is strong enough to cross the first order T-O transition line for a given initial temperature. If the transition oc-



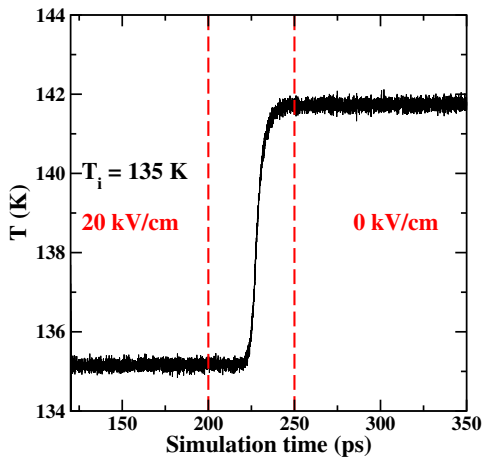


FIG. 8. Time evolution of the system temperature during a simulation for  $T_i = 135$  K, when a field of 20 kV/cm along [001] is switched off. The time period between the two red dashed lines indicates the time during which the field is slowly ramped down with a rate of  $-0.0004$  kV/cm/fs.

curs, it results in an inverse caloric temperature change of around 1 K.

For  $T_i = 125$  K, an applied field of at least 100 kV/cm is required to cross the T-O transition. However, the transition field is strongly reduced for slightly higher temperatures. For example, at  $T_i = 135$  K the T-O transition can already occur for an applied field of 20 kV/cm, and indeed we obtain essentially the same inverse temperature change as for  $T_i = 125$  K when the system undergoes the transition (see Fig. 8).

We note that in the present case, if the system is initially within the coexistence region, we initialize the system such that the application or removal of the field will result in a crossing of the transition line we want to study. However, without initial poling of the system or upon subsequent field cycling, the system may get stuck in one of the FE phases, and thus will not undergo a phase transition in subsequent field cycles. Furthermore, the system can also form complex multi-domain states,<sup>47</sup> which can, potentially, reduce the overall EC response. In practice, the limiting factor for obtaining the large EC effect related to the T-O transition entropy, is that the applied field has to be large enough to overcome the hysteretic behavior of the system, in order to reversibly drive the system back and forth between the two different phases.

#### D. Direct measurements of the EC temperature change in BTO single crystals

In order to verify the theoretical considerations and simulation results presented in the preceding subsections, we perform direct measurements of the EC temperature change in single crystals of BTO with different orientation of the crystallographic axes relative to the applied electric field (see Sec. III for details on the experimen-

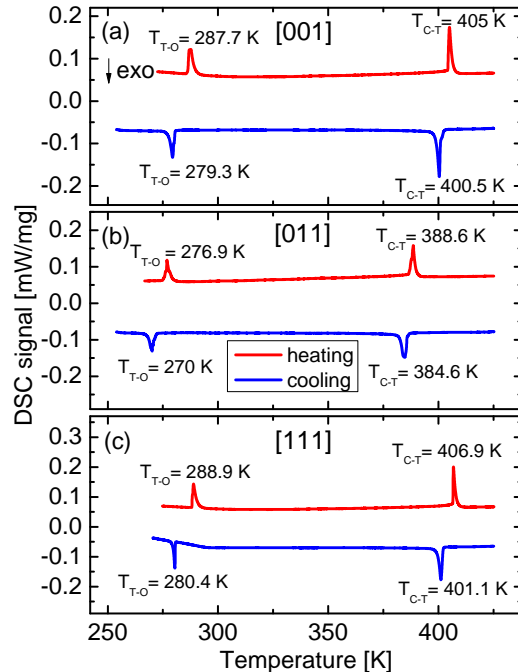


FIG. 9. Results of differential scanning calorimetry (DSC) measurements to obtain the phase transition temperatures for (a) BTO [001], (b) BTO [011], and (c) BTO [111] on cooling (blue) and on heating (red).

tal procedure). The EC measurements are performed in the vicinity of both the cubic-tetragonal (C-T) and the tetragonal-orthorhombic (T-O) phase transitions.

In Fig. 9, we first show the DSC signals measured for all BTO samples on both heating and cooling, from which the transition temperatures for the C-T and T-O transitions can be obtained. Note that in all cases, there is a thermal hysteresis of a few Kelvin between heating and cooling at both transitions. Furthermore, there is a slight shift in the transition temperatures for different BTO samples. We attribute the variation of the transition temperatures to possible variations of impurity concentration in the crystals under study.

Fig. 10 shows the measured EC temperature changes for the three BTO single crystals with different orientation near the C-T (PE-FE) phase transition. One can see that for all three orientations we obtain a positive EC effect, and the position of maximum  $\Delta T$  correlates well with the transition temperatures estimated from the DSC measurements (see Fig. 9).<sup>48</sup> Away from the phase transition region,  $\Delta T$  is significantly reduced. The largest EC temperature change is obtained for the BTO single crystal oriented along the [001] direction, with  $\Delta T_{\max} = 1.25$  K at 405 K for an applied field of 10 kV/cm. The magnitude of  $\Delta T_{\max}$  decreases for the [011]-oriented crystal (0.87 K at 388 K) and then further for the [111]-oriented sample (0.4 K around 400 K) under the same applied field. For the [001] oriented sample,

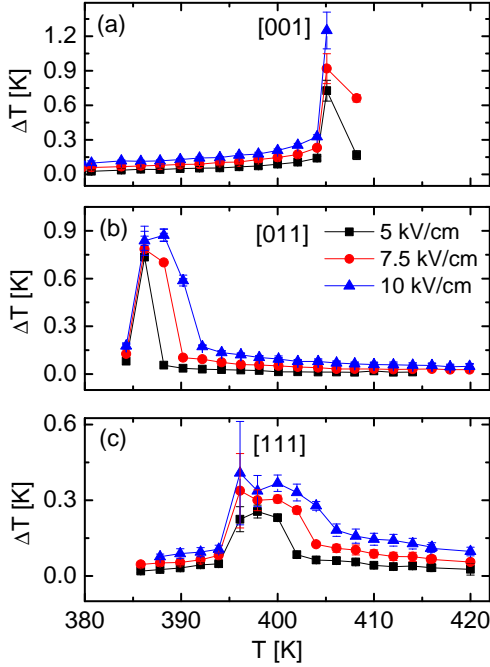


FIG. 10. Directly measured electrocaloric temperature change  $\Delta T$  for three different BTO single crystal orientations (a) BTO [001], (b) BTO [011] and (c) BTO [111] for different applied electric fields in the vicinity of the cubic-tetragonal (PE-FE) phase transition. The error bar at each point is equal to the calculated standard deviation.

measurements at temperatures  $\geq 410$  K were not possible due to large leakage currents.

This trend agrees well with what is observed in our MD simulations, i.e., for the same total applied field, the EC response is largest along [001] and smallest along [111]. Further, we note that the fact that the low temperature side of the measured EC peak is essentially field independent, whereas the high temperature side is shifted towards higher temperatures with increasing field strength, also agrees well with our simulations.

Fig. 11 depicts the EC temperature change of the three samples close to the T-O (FE-FE) phase transition. Again, the temperatures where the maximal  $\Delta T$  values can be observed are consistent with the O-T transition temperatures obtained from the DSC measurements. A normal (positive) EC effect is observed for both the [011] and [111]-oriented crystals. In contrast, an inverse (negative) EC effect occurs for the [001]-oriented crystal, which switches to a positive  $\Delta T$  for increasing temperature. The inverse EC effect in the [001] sample reaches a magnitude of  $\Delta T_{\max} = -0.06$  K for an applied electric field of 10 kV/cm in the vicinity of the transition, whereas at lower temperatures it is very small and field-independent. For the [011] and [111]-oriented crystals the EC effect reaches maximum values of  $\Delta T_{\max} = 0.12$  K and 0.24 K, respectively. We note that our current setup does not allow to cool below 273 K, and therefore we could only

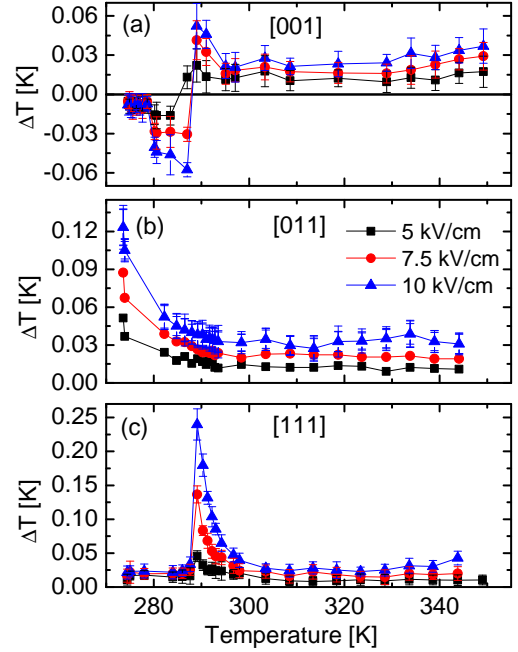


FIG. 11. Directly measured electrocaloric temperature change  $\Delta T$  for three different BTO single crystal orientations (a) BTO [001], (b) BTO [011] and (c) BTO [111] for different applied electric fields in the vicinity of the tetragonal-orthorhombic (FE-FE) phase transition.

measure the high temperature side of the  $\Delta T$  peak for the [011] sample.

The inverse response measured for the [001] sample (and the positive response for the other two orientations) is in excellent qualitative agreement with our theoretical predictions for the EC response at the O-T transition in BTO. However, quantitatively, the measured temperature changes are much smaller than what is predicted by our simulations. Furthermore, in the simulations,  $|\Delta T_{\max}|$  was rather similar for all three field directions (since it is closely related to the T-O transition entropy), whereas in the experiments  $|\Delta T_{\max}|$  varies between different field directions. These quantitative differences are most likely due to the smaller fields applied in the experiments, which are perhaps not sufficient to completely drive the system through the O-T transition. Furthermore, the presence of multiple domains in the experimentally studied samples, the influence of defects, impurities, thermal losses, etc., can in principle account for the quantitative differences between the experimental results and the simulations, which are performed for an ideal model system.

We point out that Bai, *et al.*<sup>21</sup> reported  $\Delta T = 1.4$  K under 10 kV/cm for BTO single crystals at the T-O transition, which agrees well with the magnitude of  $\Delta T$  predicted from our simulations. However, this large response was obtained only during the first field switching, and

was reduced by up to two orders of magnitude on further cycling. This is in accordance with the argument, that for small fields the system may get stuck within the coexistence region or a multi-domain configuration, reducing the overall response of the system. In our measurements, we do not observe a significant difference between first and subsequent field cycles. This could be attributed to different measurement protocols and sample histories compared to Ref. 21. However, further experiments are required to fully resolve these issues.

## V. SUMMARY AND CONCLUSIONS

In summary, we have used molecular dynamics simulations for a first principles-based effective Hamiltonian to study the EC effect in BaTiO<sub>3</sub> at all three ferroelectric transitions. Thereby, we have focused in particular on how the EC effect depends on the direction of the applied electric field relative to the crystallographic axes of BaTiO<sub>3</sub>, and we have analyzed the occurrence of an inverse EC effect at the FE-FE transitions for certain field directions. We have also performed direct measurements of the EC temperature change for BTO single crystals with electric fields applied along different crystallographic directions, in order to verify our theoretical predictions.

Our results show that there is a pronounced anisotropy of the EC effect in BaTiO<sub>3</sub>. For temperatures above the zero-field PE-FE transition temperature, i.e. where the EC effect is largest, the temperature dependence is qualitatively similar for all field directions. Nevertheless, its magnitude depends strongly on the field direction and is largest for fields applied along [001] (and crystallographically equivalent directions). This is also confirmed by our direct EC measurements on BTO single crystals.

In the temperature regions around the FE-FE transitions, the EC response exhibits pronounced qualitative differences for the different field directions. Most strikingly, an inverse EC effect is observed for certain orientations of the applied field. Using the generalized Clausius-Clapeyron equation (4), we have shown that such an inverse EC effect occurs if the electric field induces a transition from a “low entropy” towards a “high entropy” FE phase, which can happen if the polarization in the high entropy phase is oriented more favorably with respect to the applied field than in the low entropy phase. This is

indicated by a negative slope  $dE_t/dT$  of the corresponding phase transition line in the  $E$ - $T$  phase diagram, and leads to a positive jump of the polarization component along the field direction at the phase transition.

By monitoring the time evolution of polarization and temperature throughout the simulation, and by calculating  $\Delta T$  for different applied field strengths at selected temperatures, we have shown that in the simulations the inverse effect occurs exactly when the system undergoes the phase transformation and is thus intimately related to the entropy change across the phase transition. Consequently, the corresponding EC effect is only indirectly affected by the strength of the applied field, as long as it is sufficient to drive the system across the transition.

These conclusions are corroborated by direct measurements of the EC temperature change of BTO single crystals around the T-O transition, where we indeed observe an inverse EC response for fields applied along the [001] direction, whereas a normal EC effect is measured for the other two field directions ([110] and [111]). Thus, there is an overall very good qualitative correspondence between our theoretical and experimental results.

Finally, we point out the anisotropy of the EC effect is not only relevant for single crystals, but has also very important implications for measurements on polycrystalline samples. In a polycrystalline sample, different grains will have different orientations of their crystal axes relative to the applied electric field, and thus only an average over all possible orientations is measured. Furthermore, if certain orientations can even lead to an inverse EC effect, this will lead to partial cancellation and a weakening of the overall EC response. On the other hand, if the EC response is particularly strong for certain orientations, this can provide a very efficient route for optimization of the EC response by using textured polycrystalline samples, i.e. samples where certain grain orientations are preferred.<sup>49</sup>

## VI. ACKNOWLEDGMENTS

This work was supported by the Swiss National Science Foundation and the German Science Foundation (Deutsche Forschungsgemeinschaft, DFG) under the priority program SPP 1599 (“Ferroic Cooling”), project codes 200021E-162297, GR 4792/1-2, and Lu729/15. We also thank A. Planes for useful discussions.

\* madhura.marathe@mat.ethz.ch

† claude.ederer@mat.ethz.ch

<sup>1</sup> P. Kobeco and I. V. Kurtchatov, *Z. Phys.* **66**, 192 (1930).

<sup>2</sup> A. S. Mischenko, Q. Zhang, J. F. Scott, R. W. Whatmore, and N. D. Mathur, *Science* **311**, 1270 (2006).

<sup>3</sup> J. Scott, *Ann. Rev. Mater. Res.* **41**, 229 (2011).

<sup>4</sup> M. Valant, *Prog. Mater. Sci.* **57**, 980 (2012).

<sup>5</sup> Y. Liu, J. F. Scott, and B. Dkhil, *Applied Physics Reviews* **3**, 031102 (2016).

<sup>6</sup> L. Mañosa, A. Planes, and M. Acet, *Journal of Materials Chemistry A* **1**, 4925 (2013).

<sup>7</sup> X. Moya, S. Kar-Narayan, and N. D. Mathur, *Nature Materials* **13**, 439 (2014).

<sup>8</sup> S. Fähler, U. K. Rössler, O. Kastner, J. Eckert, G. Eggeler, H. Emmerich, P. Entel, S. Müller, E. Quandt, and K. Albe,

- Advanced Engineering Materials **14**, 10 (2011).
- <sup>9</sup> I. Takeuchi and K. Sandeman, *Physics Today* **68**, 4854 (2015).
  - <sup>10</sup> M. E. Lines and A. M. Glass, *Principles and Applications of Ferroelectrics and Related Materials* (Oxford University Press, 1977).
  - <sup>11</sup> S. Kar-Narayan and N. D. Mathur, *Journal of Physics D: Applied Physics* **43**, 032002 (2010).
  - <sup>12</sup> X. Moya, E. Stern-Taulats, S. Crossley, D. González-Alonso, S. Kar-Narayan, A. Planes, L. Mañosa, and N. D. Mathur, *Advanced Materials* **25**, 1360 (2013).
  - <sup>13</sup> N. Novak, R. Pirc, and Z. Kutnjak, *Phys. Rev. B* **87**, 104102 (2013).
  - <sup>14</sup> G. Akcay, S. P. Alpay, J. V. Mantese, and G. A. Rossetti, *Appl. Phys. Lett.* **90**, 252909 (2007).
  - <sup>15</sup> G. Akcay, S. P. Alpay, G. A. Rossetti, and J. F. Scott, *J. Appl. Phys.* **103**, 024104 (2008).
  - <sup>16</sup> N. Novak, Z. Kutnjak, and R. Pirc, *EPL (Europhysics Letters)* **103**, 47001 (2013).
  - <sup>17</sup> S. Beckman, L. Wan, J. A. Barr, and T. Nishimatsu, *Mater. Lett.* **89**, 254 (2012).
  - <sup>18</sup> T. Nishimatsu, J. A. Barr, and S. P. Beckman, *Journal of the Physical Society of Japan* **82**, 114605 (2013).
  - <sup>19</sup> M. Marathe and C. Ederer, *Applied Physics Letters* **104**, 212902 (2014).
  - <sup>20</sup> A. Grünebohm and T. Nishimatsu, *Phys. Rev. B* **93**, 134101 (2016).
  - <sup>21</sup> Y. Bai, K. Ding, G.-P. Zheng, S.-Q. Shi, J.-L. Cao, and L. Qiao, *AIP Advances* **2**, 022162 (2012).
  - <sup>22</sup> I. Ponomareva and S. Lisenkov, *Physical Review Letters* **108**, 167604 (2012).
  - <sup>23</sup> J. Peräntie, J. Hagberg, A. Uusimäki, and H. Jantunen, *Phys. Rev. B* **82**, 134119 (2010).
  - <sup>24</sup> G. Sebald, L. Seveyrat, D. Guyomar, L. Lebrun, B. Guiffard, and S. Pruvost, *Journal of Applied Physics* **100**, 124112 (2006).
  - <sup>25</sup> L. Luo, M. Dietze, C.-H. Solterbeck, M. Es-Souni, and H. Luo, *Applied Physics Letters* **101**, 062907 (2012).
  - <sup>26</sup> R. Chukka, S. Vandrangi, Z. Chen, L. You, J. Wang, P. Yang, and L. Chen, *AIP Advances* **3**, 072118 (2013).
  - <sup>27</sup> Y.-B. Ma, A. Grünebohm, K.-C. Meyer, K. Albe, and B.-X. Xu, *Phys. Rev. B* **94**, 094113 (2016).
  - <sup>28</sup> W. Zhong, D. Vanderbilt, and K. M. Rabe, *Phys. Rev. Lett.* **73**, 1861 (1994).
  - <sup>29</sup> W. Zhong, D. Vanderbilt, and K. M. Rabe, *Phys. Rev. B* **52**, 6301 (1995).
  - <sup>30</sup> T. Nishimatsu, M. Iwamoto, Y. Kawazoe, and U. V. Waghmare, *Phys. Rev. B* **82**, 134106 (2010).
  - <sup>31</sup> T. Nishimatsu, U. V. Waghmare, Y. Kawazoe, and D. Vanderbilt, *Phys. Rev. B* **78**, 104104 (2008).
  - <sup>32</sup> Z. Wu and R. Cohen, *Physical Review B* **73**, 235116 (2006).
  - <sup>33</sup> S. D. Bond, B. J. Leimkuhler, and B. B. Laird, *Journal of Computational Physics* **151**, 114 (1999).
  - <sup>34</sup> M. Marathe, A. Grünebohm, T. Nishimatsu, P. Entel, and C. Ederer, *Phys. Rev. B* **93**, 054110 (2016).
  - <sup>35</sup> S. Tinte, J. Íñiguez, K. M. Rabe, and D. Vanderbilt, *Phys. Rev. B* **67**, 064106 (2003).
  - <sup>36</sup> B. Rožič, B. Malič, H. Uršič, J. Holc, M. Kosec, B. Neese, Q. M. Zhang, and Z. Kutnjak, *Ferroelectrics* **405**, 26 (2010).
  - <sup>37</sup> M. Sanlialp, C. Molin, V. V. Shvartsman, S. Gebhardt, and D. C. Lupascu, *IEEE Transactions on Ultrasonics, Ferroelectrics, and Frequency Control* **63**, 1690 (2016).
  - <sup>38</sup> A. J. Bell, *Journal of Applied Physics* **89**, 3907 (2001).
  - <sup>39</sup> Y. L. Li, L. E. Cross, and L. Q. Chen, *Journal of Applied Physics* **98**, 064101 (2005).
  - <sup>40</sup> We note that for non-zero  $E_\alpha$  the distinction between PE and FE phases becomes, strictly speaking, meaningless, since there is a nonzero polarization at all temperatures. Nevertheless, we use the term “PE” to indicate the phase emanating from the zero field PE phase at high temperatures, which is still separated from the T phase at lower temperatures by a first order phase transition, at least for not too high  $E_\alpha$ .
  - <sup>41</sup> A. Planes, L. Mañosa, and M. Acet, *Journal of Physics: Condensed Matter* **21**, 233201 (2009).
  - <sup>42</sup> A. Planes, T. Castán, and A. Saxena, *Philosophical Magazine* **94**, 1893 (2014).
  - <sup>43</sup> Note that the sign convention used here for  $\Delta P$  is opposite to the one used in Ref. 41 for  $\Delta M$  and thus Eq. (4) has opposite sign compared to Eq. (11) from Ref. 41.
  - <sup>44</sup> Note that a negative slope  $dE_t/dT$  does not affect the sign of  $\Delta S$  in Eq. (4) since  $\Delta S$  depends only on the absolute value of  $dE_t/dT$ .
  - <sup>45</sup> E. Stern-Taulats, P. Lloveras, M. Barrio, E. Defay, M. Egilmez, A. Planes, J.-L. Tamarit, L. Mañosa, N. D. Mathur, and X. Moya, *APL Materials* **4**, 091102 (2016).
  - <sup>46</sup> G. Shirane, H. Danner, A. Pavlovic, and R. Pepinsky, *Physical Review* **93**, 672673 (1954).
  - <sup>47</sup> T. Limboeck and E. Soergel, *Applied Physics Letters* **105**, 152901 (2014).
  - <sup>48</sup> We note that there is often a discrepancy between transition temperatures estimated using different methods. This can be related to differences in experimental setups such as the rate of temperature change, the position of the temperature sensor relative to the sample, etc.
  - <sup>49</sup> F. L. Goupil, A.-K. Axelsson, L. J. Dunne, M. Valant, G. Manos, T. Lukasiewicz, J. Dec, A. Berenov, and N. M. Alford, *Advanced Energy Materials* **4**, 1301688 (2014).